INDONESIAN JOURNAL ON GEOSCIENCE
Geological Agency
Ministry of Energy and Mineral Resources

Journal homepage: http://ijog.geologi.esdm.go.id
ISSN 2355-9314, e-ISSN 2355-9306

Characterization of Rare Earth Elements in Cassiterite-Associated Minerals in Bangka-Belitung Islands, Indonesia

Syafrizal[1], Arie Naftali Hawu Hede[1], Tomy Alvin Rivai[1,2], and Rudy Fernando Sihite[3]

[1]Earth Resource Exploration Research Group, Faculty of Mining and Petroleum Engineering, Bandung Institute of Technology, Indonesia, 40132
[2]Geological Survey of Japan, National Institute of Advanced Industrial Science and Technology, Central-7 1-1-1 Higashi, Tsukuba 305-8567, Japan
[3]Department of Production and Industrial Technology, Sumatera Institute of Technology

Corresponding author: syafrizal@itb.ac.id
Manuscript received: November, 19, 2021; revised: January, 24, 2024;
approved: June, 19, 2024; available online: July, 8, 2024

Abstract - Rare earth elements (REEs) are crucial to numerous industries of high-technology as raw materials. The growth of a long-term relationship between REE supply and demand to develop hi-tech industries is becoming tight in the world market, while the mineral supply chain is being distorted by COVID-19. The availability of information and data regarding the REE resource potential and characteristics are interesting research subjects to examine its economic value as alternative sources. This research aims to provide basic information about the existence and characteristics of REEs in cassiterite-associated minerals located in Bangka and Belitung Islands. Fifty-one samples consisting of primary deposits, placer deposits, concentrates, and tailings were collected from the southern Bangka and Belitung region. The samples were analyzed using microscope, x-ray diffraction (XRD), scanning electron microscopy (SEM), electron probe micro-analysis (EPMA), and inductively coupled plasma mass spectrometry (ICP-MS). The results show that the REE-bearing minerals comprised monazite and xenotime. Monazite, the most dominant REE-bearing mineral, contains light REEs (Ce-dominant), while xenotime contains heavy REE (Y-dominant). The results of SEM with energy-dispersive spectroscopy show that monazite contains other LREE (La and Nd), and xenotime also contains other HREE (Dy and Yb). Moreover, zircon and ilmenite can be considered as economical cassiterite-associated minerals that have other mineral inclusion, but have no REE contain.

Keywords: monazite, xenotime, REE, cassiterite-associated mineral, Bangka-Belitung Islands

© IJOG - 2024

How to cite this article:
Syafrizal, Hede, A.N.H., Rivai, T.A., and Sihite, R.F., 2024. Characterization of Rare Earth Elements in Cassiterite-Associated Minerals in Bangka-Belitung Islands, Indonesia. *Indonesian Journal on Geoscience*, 11 (2), p.201-219. DOI: 10.17014/ijog.11.2.201-219

Introduction

Background

Rare earth elements (REEs) consist of fifteen elements of the lanthanide group (La–Lu), scandium (Sc), and yttrium (Y) (Connelly *et al*., 2005). Commonly, the REEs are grouped based on their atomic weight into light REE (LREE) and heavy REE (HREE) (Gosen *et al*., 2017). The LREE group encompasses elements with atomic numbers of 57–64 (La–Gd), while the HREE group includes elements with atomic numbers of 65–71 (Tb–Lu). Even though Y has a light atomic number of 39, it belongs to the HREE group because of its physical and chemical similarities to other HREEs, particularly its ionic radius, which is nearly identical to that of Ho (Chakhmouradian and Wall, 2012). REEs, which have high economic value and play a significant role in the development of advanced technology, are considered among the most stra-

tegic commodities in the 21st century (Zhou *et al*., 2017). The dependence of modern civilization on REEs is illustrated by the increased demand for them, which is projected to be sustained at least over the coming decades (Barakos *et al*., 2016; Haque *et al*., 2014). There were two main problems along with REE supply in world market. First about China dominance which supplies approximately 58 % of the world rare earth oxide (REO) demand and secondary the global supply disruption which have been limited during the COVID-19 pandemic (USGS, 2021; Zglinicki *et al*., 2021). The unstable REE supply enforces the exploration programme for alternative critical mineral sources. A proven way to increase the supply of REE minerals is to cultivate the mining of the cassiterite-associated mineral that contained REEs generated during the mining of cassiterite-bearing sands in Bangka and Belitung Islands (Szamałek *et al*., 2013). This option is to complement other options that have been studied regarding REE mineralization in Lingga laterite profile, Sulawesi laterite profile, and REE potential in tin waste dump on Singkep Island (Irzon, 2021; Irzon *et al*., 2016; Maulana *et al.,* 2016).

A study estimated the Bangka and Belitung Islands to contain approximately 471 million m^3 of hypothetical monazite resources (Aryanto and Kamiludin, 2016). The observed LREE enrichment aligns with monazite preference for incorporating LREEs due to their compatible ionic radii and charge (Syafrizal *et al*., 2017). Additionally, placer deposit formation processes favour LREE-bearing minerals due to their resilience against weathering (Kudrass, 2016). However, the negative issue is dealing with the high contents of radioactive elements (thorium and uranium), which become impurities and affect higher REO extraction costs (Zglinicki *et al*., 2021). Nevertheless, the Indonesian government committed to develop the high-tech processing infrastructure to join the global REE market as a supplier (Mcbeth, 2020). This commitment is supported by the Indonesian omnibus law on job creation, specifically Article 9, which allows state-owned enterprises to collaborate with private companies to mine associated radioactive minerals (Indonesia, 2020).

Bangka-Belitung is known as the largest tin-producing region in Indonesia. The islands are traversed by the Southeast Asian tin belt, which covers an area of >3,000 km extending from Myanmar to Indonesia (Ng *et al*., 2017). The belt is composed of various granite plutons, which can be divided into three groups: The Main Range Province, The Eastern Province, and The Western Province (Figure 1) (Cobbing *et al*., 1986; Ng *et al*., 2017). Significant tin mineralization occurs mainly in The Main Range Province, with minor occurrences in the Eastern and Western Provinces (Schwartz *et al*., 1995). Tin minerals are primarily cassiterite; additionally, there are minor occurrences of malayaite, stannite, stannoidite, and ixiolite (Schwartz *et al*., 1995). The term cassiterite-associated minerals refer to those minerals, such as ilmenite, monazite, xenotime, and zircon that occur alongside cassiterite in Bangka-Belitung tin deposits, but may not directly contribute to tin production. These minerals are of significant interest due to their potential for containing valuable REEs, with monazite and xenotime being particularly important REE-bearing minerals within this group (Firdaus *et al*., 2020; Purwadi *et al*., 2019; Suprapto, 2009). This study aims to investigate the occurrence and characteristics of REEs within cassiterite-associated minerals in The Bangka and Belitung Islands, contributing to the assessment of their potential as REE resources.

Geological Setting

The Bangka and Belitung Islands, also known as The Indonesian Tin Islands, are primarily composed of granites from two distinct provinces. The Eastern Province features Early Permian-Late Triassic I-type granites, while predominantly Late Triassic S-type granites characterize The Main Range Province (Cobbing *et al*., 1986). The extensive distribution of granites in Bangka-Belitung were formed during hydrothermal and metasomatic processes, enriched by cassiterite mineralization and its associated minerals such as allanite, titanite, apatite, zircon, monazite,

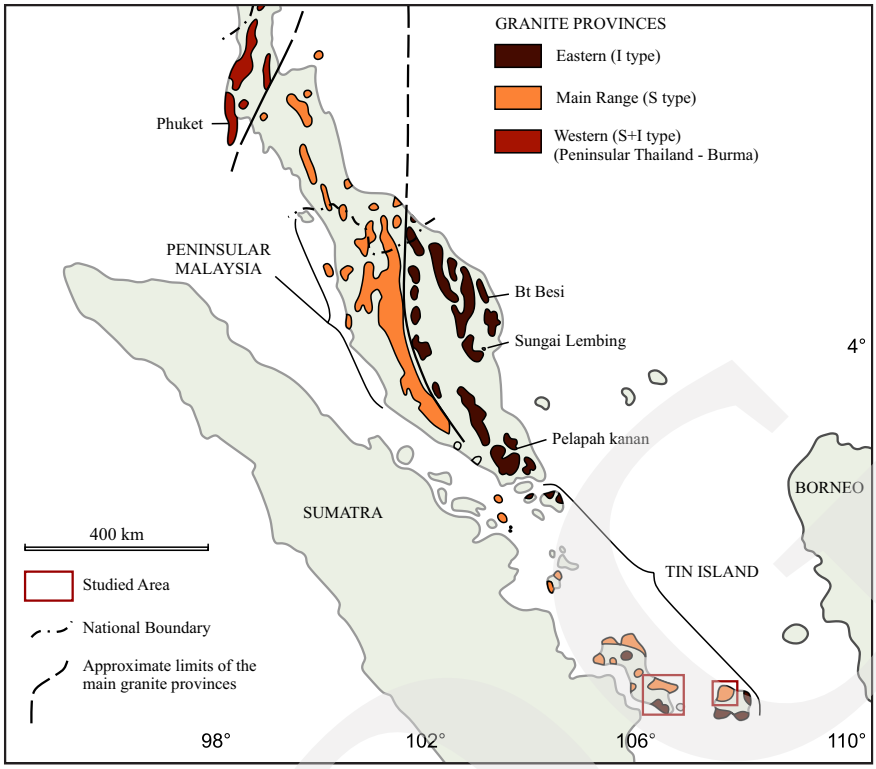

Figure 1. Segment of the Southeast Asian Tin Belt highlights the southern section, featuring the islands of Bangka and Belitung within the Main Range and Eastern Granite Provinces (Cobbing *et al.*, 1986; Ng *et al.*, 2017).

xenotime, ilmenite, and Th silicates (Cobbing *et al.*, 1986; Schwartz *et al.*, 1995; Zglinicki *et al.*, 2022). Over time, the granites have undergone intensive chemical and mechanical weathering under tropical climatic conditions, leading to their increased susceptibility to erosion (Riebe *et al.*, 2001). The resulting weathering products have accumulated as secondary deposits (Sengupta and Gosen, 2016). Two types of REE secondary deposits are placer and ion-adsorption clay, which formed from weathering products of granitic rocks with abundant REE content (Yaraghi *et al.*, 2020).

The oldest rock in southern Bangka is the Permo-Carboniferous Pemali Metamorphic Complex, which consists of phyllite, schist, and quartzite (Margono *et al.*, 1995). The complex is unconformably overlain by the Triassic Tanjunggenting Formation, composed of interbedded sandstone and claystone with local occurrences of limestone lenses. The sedimentary sequence was intruded by the Klabat biotite granite, granodiorite, adamelite, diorite, and quartz diorite, which are classified into I-type (igneous) and S-type (metasedimentary) (Schwartz and Surjono, 1991). The Late Miocene – Early Pleistocene Ranggam Formation (interbedded sandstone, claystone, and conglomerate) occurs in the northern area (Figure 2a).

The basement of Belitung Island is made up of the Kelapa Kampit and Tajam Formations (Figure 2b) (Baharrudin and Sidarto, 1995; Jones *et al.*, 1977). The Kelapa Kampit Formation comprises folded metasandstone interbedded with slate, mudstone, shale, tuffaceous siltstone, and chert. The Tajam Formation is composed of quartz sandstone with intercalation of siltstone. The two formations showan interfingering structure. Fossils in both formations suggest the Permo-Carboniferous deposition period (Jones *et al.*, 1977). Basaltic lava and volcanic breccia of the same age are grouped into Siantu Formation. In northern Belitung, granitic magmatism took place during Triassic, producing a large granitic body known as Tanjungpandan Granite, which covers an area of 900 km^2 (Baharrudin and Sidarto, 1995; Schwartz and Surjono, 1990). Along with granite from Bangka Island, granites from Belitung Is-

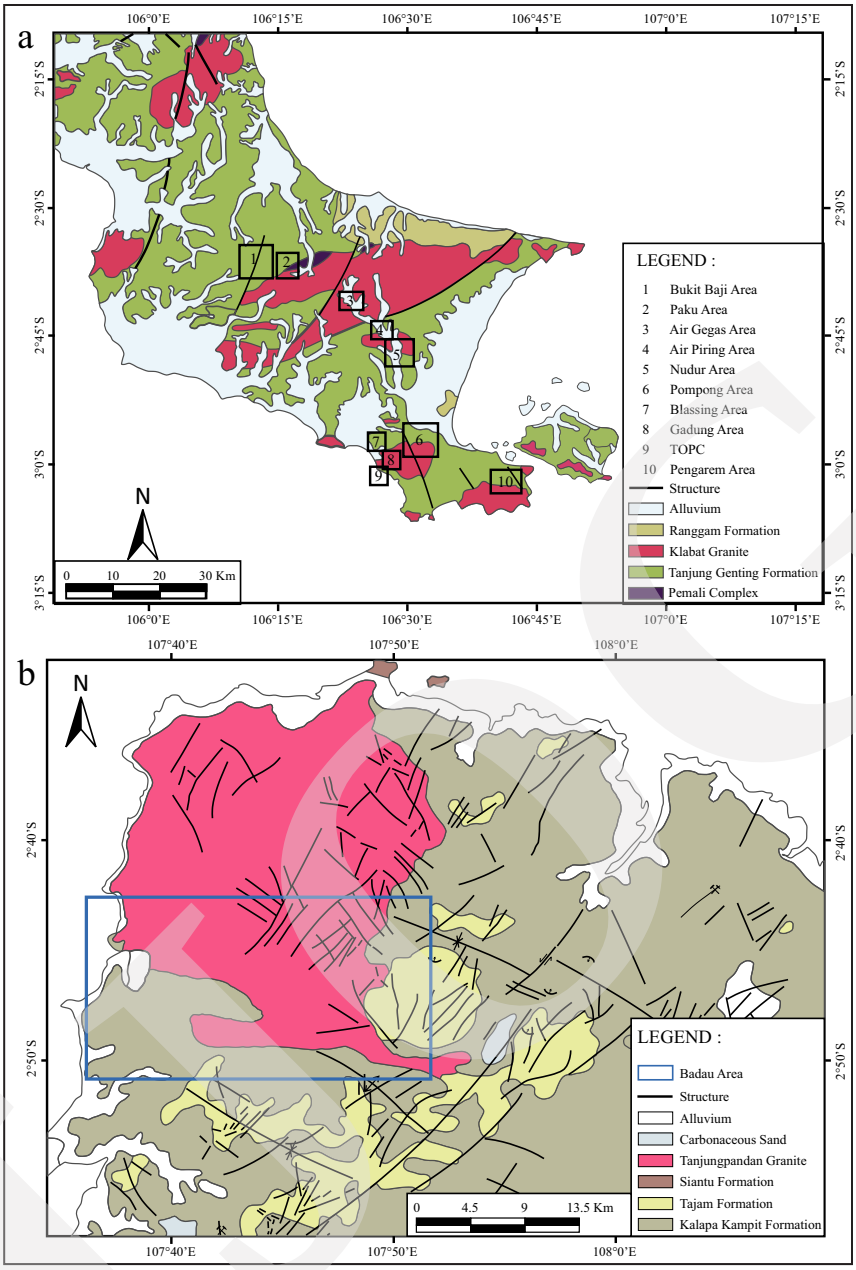

Figure 2. Regional geology map of (a) Southern Bangka (Margono *et al*., 1995) and (b) Belitung (Baharrudin and Sidarto, 1995). Black boxes mark sampling areas in southern Bangka, while blue boxes highlight those in Belitung.

land are classified into S-type (metasedimentary) and I-type (igneous) (Jones *et al*., 1977; Schwartz and Surjono, 1990).

Methods and Materials

Fifty-one samples were collected from various locations in southern Bangka and Belitung, including active mining operations, abandoned mining sites, and greenfield exploration areas (Table 1). The samples represent primary deposits, placer deposits in cassiterite-bearing sands, heavy mineral concentrates from both primary processing using sluice boxes and secondary processing at a tin ore processing centre (Pusat Pengolahan Bijih Timah, PPBT, in Indonesian) and tailings. The processing of cassiterite-bearing sands has several stages that result concentrates and tailings in each stage. The primary deposit

Table 1. List of Samples from Southern Bangka and Belitung. Coordinates and statutes are listed for each site alongside the type of sample and analysis method performed for each sample

Area	Sample code	Coordinate		Location	Mine Status	Type of deposit/ sample	Type of laboratory analysis				
		Latitude	Longitude				Microscopic	XRD	SEM	EPMA	ICP-MS
South Bangka	BA-PR-1	-3,0241	106,6932	Pangarem	Active	Primary	✓	✓	✓	✓	✓
	BA-PR-2	-2,9742	106,4691	Gadung	Active	Primary	✓	✓			
	BA-PR-3	-2,5999	106,2104	Bukit Baji	Active	Primary	✓	✓			
	BA-AL-1	-2,9372	106,5262	Pompong	Active	Placer	✓	✓			✓
	BA-AL-2	-2,7700	106,4774	Nudur	Active	Placer	✓	✓			
	BA-AL-3	-2,7652	106,4688	Nudur	Active	Placer	✓	✓			
	BA-AL-4	-2,7490	106,4642	Nudur	Abandoned	Placer	✓	✓			
	BA-AL-5	-2,7488	106,4643	Nudur	Abandoned	Placer	✓	✓			
	BA-AL-6	-2,5966	106,2184	Bukit Baji	Abandoned	Placer	✓	✓			
	BA-AL-7	-2,6035	106,2668	Paku	Abandoned	Placer	✓	✓			
	BA-CL-1	-2,9553	106,5278	Pompong	Active	Placer	✓	✓		✓	✓
	BA-CNS-1	-3,0103	106,4427	PPBT*	-	Concentrate	✓	✓	✓	✓	✓
	BA-CNS-2	-3,0103	106,4427	PPBT*	-	Concentrate	✓	✓	✓	✓	
	BA-CNS-3	-2,7693	106,4759	Nudur	Active	Concentrate	✓	✓			
	BA-CNS-4	-2,5996	106,2132	Bukit Baji	Active	Concentrate	✓	✓			
	BA-TL-1	-2,9269	106,5242	Pompong	Abandoned	Tailing	✓	✓			
	BA-TL-2	-2,9359	106,5245	Pompong	Abandoned	Tailing	✓	✓			✓
	BA-TL-3	-2,9386	106,5245	Pompong	Active	Tailing	✓	✓			
	BA-TL-4	-3,0241	106,6932	Pengarem	Active	Tailing	✓	✓			
	BA-TL-5	-3,0250	106,6961	Pengarem	Abandoned	Tailing	✓	✓			
	BA-TL-6	-2,9738	106,4670	Gadung	Active	Tailing	✓	✓			
	BA-TL-7	-2,9681	106,4501	Blasing	Active	Tailing	✓	✓			
	BA-TL-8	-2,7676	106,4755	Nudur	Active	Tailing	✓	✓			
	BA-TL-9	-2,7527	106,4621	Nudur	Abandoned	Tailing	✓	✓			
	BA-TL-10	-2,6736	106,3880	Air Gegas	Abandoned	Tailing	✓	✓			
	BA-TL-11	-2,5989	106,2142	Bukit Baji	Active	Tailing	✓	✓			✓
	BA-TL-12	-2,6039	106,2676	Paku	Abandoned	Tailing	✓	✓			
Belitung	BL-PR-2	-2,7657	107,7999	Badau	Greenfield	Primary	✓	✓			✓
	BL-PR-3	-2,7387	107,8176	Badau	Greenfield	Primary	✓	✓			✓
	BL-EL-1	-2,7371	107,8295	Badau	Greenfield	Placer	✓	✓			✓
	BL-CL-1	-2,7318	107,7985	Badau	Greenfield	Placer	✓	✓			✓
	BL-AL-1	-2,8286	107,7345	Badau	Active	Placer	✓	✓			✓
	BL-AL-2	-2,8286	107,7345	Badau	Active	Placer	✓	✓			✓
	BL-AL-3	-2,8286	107,7345	Badau	Active	Placer	✓	✓			
	BL-AL-4	-2,8286	107,7345	Badau	Active	Placer	✓	✓			
	BL-AL-5	-2,8020	107,7634	Badau	Active	Placer	✓	✓			✓
	BL-AL-6	-2,8020	107,7634	Badau	Active	Placer	✓	✓			
	BL-AL-7	-2,7654	107,7723	Badau	Greenfield	Placer	✓	✓			
	BL-EP-1	-2,7419	107,6242	Badau	Abandoned	Placer	✓	✓			
	BL-EP-2	-2,7613	107,6116	Badau	Abandoned	Placer	✓	✓			
	BL-TLS-1	-2,8000	107,7653	Badau	Active	Tailing	✓	✓			
	BL-TLS-2	-2,8291	107,7360	Badau	Active	Tailing	✓	✓			✓
	BL-TLS-3	-2,8295	107,7356	Badau	Active	Tailing	✓	✓			✓
	BL-TL-1	-2,8034	107,7602	Badau	Active	Tailing	✓	✓			✓
	BL-TL-2	-2,8038	107,7590	Badau	Active	Tailing	✓	✓			✓
	BL-TL-3	-2,7980	107,7665	Badau	Active	Tailing	✓	✓			
	BL-TLL	-2,7988	107,7660	Badau	Active	Tailing	✓	✓			✓
	BL-CNS-1	-2,7988	107,7660	Badau	Active	Concentrate	✓	✓			✓
	BL-CNS-2	-2,8018	107,7598	Badau	Active	Concentrate	✓	✓	✓	✓	
	BL-CNS-3	-2,8018	107,7598	Badau	Active	Concentrate	✓	✓	✓	✓	✓

Tin ore processing center (Pusat Pengolahan Biji Timah, PPBT, in Indonesian)

samples were obtained using chip-sampling method, while the other samples were collected using grab-sampling method.

The samples were sieved with sizes 48 mesh, 65 mesh, and 100 mesh at the Laboratory of Material Processing in Bandung Institute of Technology. Selected samples were observed under Nikon binocular for grain counting analysis. The samples were subjected to mineralogical observations and were observed by using Nikon microscope ECLIPSE LV100N POL, X-ray diffraction (XRD, Rigaku Multiflex), scanning electron microscopy (SEM, JEOL JSM-6610LV), and electron probe micro-analysis (EPMA, JXA-8230). REE contents were analyzed using inductively coupled plasma-mass spectrometry (ICP-MS, Agilent 7500ce) at Kyushu University, Japan. Sample solutions for ICP-MS analysis were dissolved by acid leach (HF, $HClO_4$, and HNO_3). XRD, SEM, and EPMA examinations were completed at the Laboratory of Economic Geology in Akita University, Japan. Meanwhile, the grain counting analysis and microscope observations were analyzed at the Laboratory of Mineralogy and Geochemistry in Bandung Institute of Technology.

Samples were crushed and pulverized to less than 200 mesh. The cassiterite-associated minerals and REE-bearing minerals were identified by XRD analysis, and the diffractograms were recorded in the 2° to 65° angle range with CuKα radiation. The polished samples were coated with 30 nm thin carbon film—the qualitative and quantitative analyses to detail characteristics of the REE-bearing minerals by using SEM equipped with back scattered electron (BSE) and energy dispersive spectrometer (EDS) detectors, and EPMA analyses. The standard materials used to calibrate the EPMA measurement were NdP_5O_{14}, CeP_5O_{14}, LaP_5O_{14}, and $ZrYO_2$ based on the targeted minerals (monazite, xenotime, and zircon) which contained those materials. The analytical time of EPMA for peak and background was 40 and 20 seconds. The preparation and analysis of REEs using ICP-MS followed established protocols similar to those described in Akagi *et al*. (2011), including correction for potential BaO interference on Eu. Calibration involved multi-element standards with concentrations ranging from 0.05 to 50 µg/l depending on the specific REE, ensuring accurate quantification within the expected range of the samples.

Results

Mineralogy

Microscope observation reveals a variety of minerals within the studied area, including quartz, ilmenite, hematite, magnetite, cassiterite, zircon, rutile, tourmaline, muscovite, monazite, and xenotime. Within the granite matrices, predominant minerals include K-feldspar, plagioclase, quartz, biotite, sericite, and chlorite. Notably, accessory minerals such as apatite, monazite, xenotime, zircon, and ilmenite are identified, exhibiting distinct textural and compositional characteristics within the granite matrices (Figure 3a). Minerals commonly associated with cassiterite, such as ilmenite, zircon, monazite, and xenotime are concentrated mostly in the sand to silt-sized particles, and often exhibit a high degree of liberation. Figure 3b details the fine-grained distribution of monazite and xenotime, showcasing their range of angular to rounded grain shapes. The degree of liberation of these minerals was commonly high.

Monazite and xenotime contain REEs and radioactive elements which can induce radioactive decay and damage the mineral structure, creating cracks and increasing their susceptibility to weathering by aqueous solutions such as rainwater or groundwater. Field observation and laboratory analysis indicated no REE-bearing minerals like allanite, apatite, titanite in the alluvial, concentrate, and tailing samples. It could be related to those minerals that are easily dissolved in weathering fluids (Sanematsu and Watanabe, 2016). Table 2 displays grain counting results and summarizes mineral proportion in each sample type, normalized to all the cassiterite-associated minerals observed. Irrespective of sample types, cassiterite grains are dominant in the 48 mesh frac-

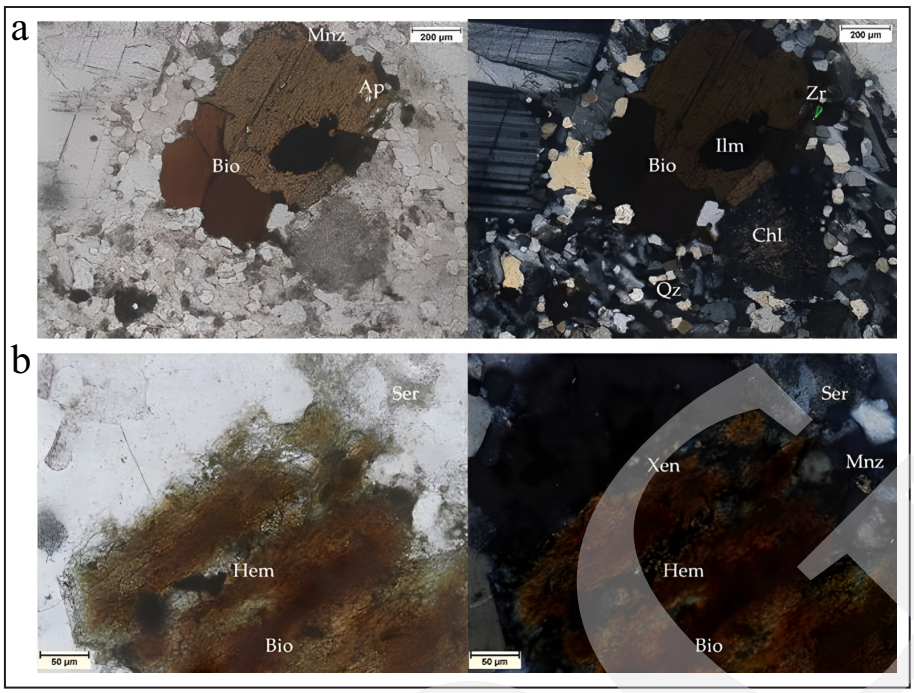

Figure 3. Photomicrographs of southern Bangka granite (BA-PR-1) under parallel nicol (left) and cross nicol (right). (a) Monazite, apatite, and ilmenite are present as inclusions in biotite. Zircon is embedded in quartz. (b) Abundant fibrous hematite and fine-grained monazite and xenotime in biotite. Abbreviation: Bio (biotite), Ap (apatite), Mnz (monazite), Zr (zircon), Ilm (ilmenite), Chl (chlorite), Qtz (quartz), Xen (xenotime), Hem (hematite), Ser (sericite).

Table 2. Normalized Average Mineral Composition (% vol.) Based on Grain-counting Analysis

Location	Deposit	Fraction	Mineral			
			Cassiterite (% vol.)	Monazite - xenotime (% vol.)	Ilmenite (% vol.)	Zircon (% vol.)
South Bangka	Placer	#48	46.37	0	47.02	6.62
		#65	24.97	3.96	56.93	14.14
		#100	50.43	5.07	21.48	23.02
	Concentrate	#48	94.28	1.75	3.97	0
		#65	86.71	3.8	2.22	7.27
		#100	45.12	12.57	11.72	30.59
	Tailing	#48	77.71	2.47	9.98	9.83
		#65	62.51	3.99	5.14	28.35
		#100	56.76	4.88	4.9	33.46
Belitung	Placer	#48	80.67	18.4	0.23	0.7
		#65	25.32	30.87	8.16	35.65
		#100	4.78	11.55	2.35	81.32
	Concentrate	#48	48.86	17.98	32.79	0.37
		#65	35.2	15.61	49.03	0.15
		#100	30.9	22.21	43.02	3.87
	Tailing	#48	39.73	27.94	14.74	17.59
		#65	45.67	23.61	11.59	19.14
		#100	21.07	16.94	5.8	56.19

tion. Its content ranges from 40 to 95 % vol. The dominance of cassiterite extends to other fractions in Bangka concentrates and tailings, whereas in Belitung, it is less abundant than ilmenite. Monazite and xenotime occur at lower abundances on Bangka Island (less than 12 % vol.) compared to those found in Belitung Island samples, which contain 12 to 31 % vol. monazite and xenotime.

XRD Analysis

Figure 4 presents the representative powder X-ray diffraction patterns of four sample types. Three samples from primary, placer, and tailing (Figures 4a-b, d) show similar peak patterns but different intensity levels for each mineral. The primary sample of granite (Figure 4a) is composed of quartz, biotite, albite, cassiterite, monazite, and xenotime. Ilmenite was found in the alluvial sample (Figure 4b), along with monazite and quartz. The concentrate sample has a lower intensity than the other samples, but shows monazite, ilmenite, xenotime, and cassiterite peaks. The tailing sample (Figure 4d) was dominated by the quartz sample and the least of monazite peaks. The concentrate sample (Figure 4c) is characterized by a few peaks of cassiterite and other heavy minerals. Additionally, it is hard to identify by XRD method due to the dense peak of quartz. The light density of quartz (± 2.6 g/cm^3) and hardness of quartz are two of the factors that allow this mineral to be transported and accumulated away from its primary source (Gosen *et al*., 2017; Sengupta and Gosen, 2016).

The concentrate sample diffractograms are different from those of other samples, probably due to the high amount of iron oxides, such as ilmenite, magnetite, and hematite, which can reduce the X-ray penetration (Mos *et al*., 2018). Moreover, the quartz proportion was detected in the tailing samples up to 90 %, indicated the efficiency of the cassiterite concentration process. All the samples have been indicated by the presence of cassiterite-associated minerals, that monazite and xenotime were the common peaks, followed by ilmenite. A high content of heavy minerals was detected at concentrate samples,

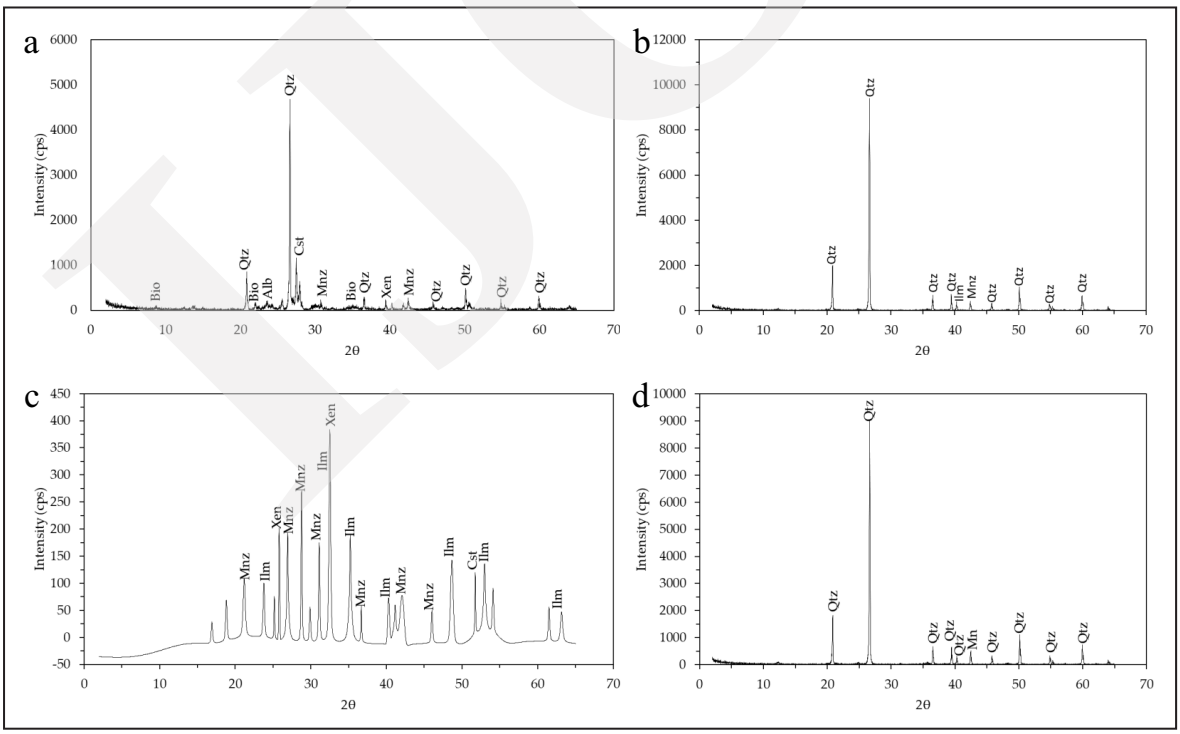

Figure 4. Examples of the diffractograms of the (a) Primary (BL-PR-2), (b) Placer (BA-AL-2), (c) Concentrate (BL-CNS-3), and (d) Tailing samples (BA-TL-7). Abbreviation: Bio (biotite), Qtz (quartz), Alb (albite), Cst (cassiterite), Mnz (monazite), Xen (xenotime), Ilm (ilmenite).

indicating that cassiterite extraction recovery is up to 74 %. In addition, numerous occurrences of REE-bearing minerals (monazite and xenotime) at the concentrate samples have been confirmed by mineralogical observations.

SEM Analysis

Based on the microscopic observation and XRD analysis, the concentrate samples contained significant cassiterite-associated mineral contents, including REE-bearing minerals. Thus, the concentrate samples were selected for SEM analysis. The back-scattered electron (BSE) images display the weak structures (fractures and cavities) in the REE-bearing minerals. For example, the monazite from Belitung (BL-CNS-2) has abundant Th at point 3 of 74.93 % wt. ThO_2 as solid inclusion through semiquantitative analysis (Figure 5a and Table 3). The metamorphism is able to break down monazite to Th-rich minerals in the monazite-huttonite series (Kelly *et al*., 2012). The subhedral monazite has slight scratches and fractures, and it may have lost its crystalline structure owing to the Th radioactive decay. EDS measurements presented semiquantitative content at point 1 of 32.78 % Ce_2O_3, 15.5 % of La_2O_3, and 10.04 % of Nd_2O_3. This point demonstrated that among the lanthanide elements in monazite grain, cerium, lanthanum, and neodymium are always predominant over the others.

Additionally, the xenotime grain very scarce in the concentrate sample. The BSE image shows the large anhedral xenotime present in the fine fractions (65 mesh and 100 mesh) (Figure 5b). It has an elongated (cylindrical) shape which makes it pass at the fine mesh. Based on the EDS analysis, the xenotime has no actinide concentration and has no intensive cracks. Xenotime at point 1 has been dominated by lanthanide elements of Y_2O_3, Dy_2O_5, and Yb_2O_6, respectively (Table 3). In contrast to the weight percent at dark point 2 within the grain which has low Y_2O_3 and Dy_2O_5 content, but higher Yb_2O_6 up to 26.52 % and SiO_2 up to 70.9 %. Semiquantitative analysis has proven that the dark point is the silicate impurities in the xenotime cavity.

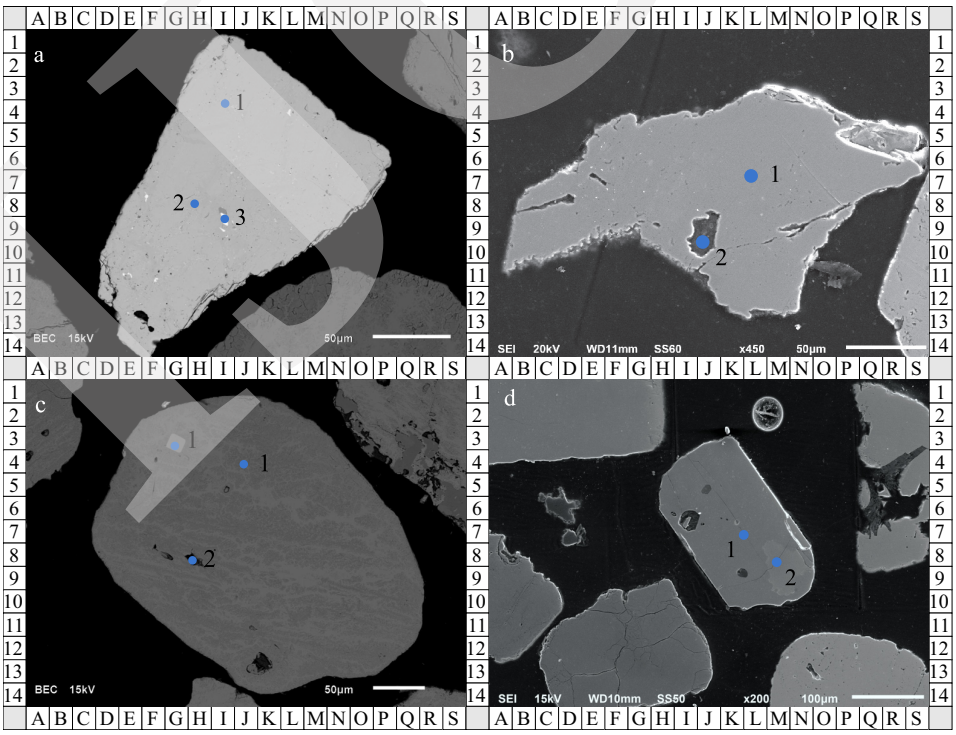

Figure 5. BSE images of mineral samples from Belitung (BL-CNS-2) showing (a) Monazite and (b) Xenotime, along with (c) Ilmenite from the same location, and (d) Zircon from southern Bangka (BA-CNS-2). Blue points mark the analytical spots for semiquantitative analysis detailed in Table 3.

Table 3. SEM-EDS of Semiquantitative Analyses of Monazite, Xenotime, Ilmenite, and Zircon

Mineral		**Monazite**	
Sample ID		**BL-CNS-2**	
Point of analysis (mineral)	1 (monazite)	2 (ferro-silicate)	3 (huttonite)
% wt			
Ce_2O_3	32.78	-	-
La_2O_3	15.5	-	-
Nd_2O_3	10.04	-	-
ThO_2	5.94	-	74.93
P_2O_5	34.04	2.5	2.03
SiO_2	1.69	26.46	23.05
FeO	-	49.02	-
Al_2O_3	-	15.7	-
K_2O	-	6.33	-
Total	**100**	**100**	**100**
Mineral		**Xenotime**	
Sample ID		**(BL-CNS-2)**	
Point of analysis (mineral)	1 (xenotime)	2 (silicate)	-
P_2O_5	40.57	1.08	-
Y_2O_3	49.61	1.25	-
Dy_2O_5	5.58	0.26	-
Yb_2O_6	4.24	26.52	-
SiO_2	-	70.9	-
Total	**100**	**100**	**-**
Mineral		**Ilmenite**	
Sample ID		**BL-CNS-2**	
Point of analysis (mineral)	1 (zircon)	2 (ilmenite)	3 (ilmenite)
FeO	-	30.97	33.06
TiO_2	-	64.49	62.07
SiO_2	31.46	-	-
ZrO_2	68.54	-	-
MnO	-	4.54	4.86
Total	**100**	**100**	**100**
Mineral		**Zircon**	
Sample ID		**(BL-CNS-3)**	
Point of analysis (mineral)	1 (zircon)	2 (zircon)	-
ZrO_2	67.79	67.74	-
SiO_2	32.21	32.26	-
Total	**100**	**100**	**-**

BSE image reveals the mineral texture of the ilmenite (Figure 5c) from a concentrate sample comprised solid exsolution texture and dark-light zoning lamellae. It is probably due to the presence of Ti- and Fe- rich portions, approximately 65 % and 35 %, respectively. Darker parts of ilmenites are characterized by a greater content of Fe in contrast to brighter parts. Ilmenite from southern Bangka samples has higher Fe and lower Ti rather than Belitung samples. In addition, the anhedral ilmenite also has zircon inclusion at point 1, such as a tiny bright grain which was identified as the presence of 68.54 % ZrO_2 and 31.46 % SiO_2 (Table 3). However, zircon grains from the southern Bangka samples (Figure 5d) had fractured intensively than those from the Belitung samples. The zircon from the Belitung sample also has intergrowth zoning. Using SEM-energy dispersive spectroscopy (EDS), it was determined that the Zr concentration in the dark zone was higher than that in the light zone. In addition, all the zircon observed on polished samples had very low REE content, in amounts of below detection limit 0.1 % wt. each for the Y_2O_3, Ce_2O_3, and La_2O_3 elements, which can not be detected.

EPMA Analysis

A total of four concentrate samples were selected for EPMA analysis to increase the likelihood of finding targeted minerals, each two of southern Bangka and Belitung. Table 4 shows EPMA results of concentrate samples. The EPMA analysis focused on specific elements relevant to the study objectives, and did not include a comprehensive analysis of all elements present in the minerals. Therefore, the total percentages do not represent 100 % of the mineral composition. The mineral contains zirconium oxides ranging from 62.40 % wt. to 66.03 % wt. with no REEs detected. Only major elements (Zr and Si) were analyzed with additional elements of interest (Al, Ca, Fe, Y, and Ce), thus making the range of total percent weight of 86.39-96.8 %. The stoichiometric calculation was carried out by weight percent to determine the atoms per formula unit (a.p.f.u.). The basis used for this stoichiometric normalization depends on the amount of oxygen in the ideal chemical formula. Ideally, the zircon chemical formula is $ZrSiO_4$. Based on the EPMA results, zircon got additional elements, such as Fe, Ca, and Al, but these elements appeared to have low percentage weights (Figure 6a). This analysis demonstrates that zircon has empirical formula $Zr_{1.04}Si_{0.95}O_4$, $Zr_{1.06}Si_{0.94}O_4$, $Zr_{1.04}Si_{0.95}O_4$, and $Zr_{1.03}Si_{0.98}O_4$.

Monazite contains high contents of Ce and La, and some minor elements were detected, *i.e*. Nd, P, Si, Al, and Fe. The empirical formulas of the analyzed monazite are $Ce_{0.23}La_{0.18}Si_{0.05}Al_{0.01}P_{1.31}O_4$ and $Ce_{0.31}La_{0.22}Si_{0.03}P_{1.26}O_4$. Hence, the monazite-(Ce) is the preferred name, because the Ce is always greater than other lanthanide group elements in monazite (Figure 6b). Except for Fe and Ti, ilmenite in the southern Bangka and Belitung hosted Mn, Al, Mg, and Si (Figure 6c). Its empirical formulas are $Fe_{0.89}Al_{0.15}Si_{0.1}Mg_{0.05}Mn_{0.02}Ti_{0.81}O_3$, $Fe_{0.81}Mn_{0.1}Ti_{1.03}O_3$, and $Fe_{0.87}Mn_{0.1}Ti_{1.01}O_3$. In southern Bangka, the mineral has an average of 39.5 % wt. FeO and 50.94 % wt. TiO_2. However, the FeO and TiO_2 in ilmenite from Belitung were

Table 4. EPMA Analysis of Concentrate Samples Principal Oxide weights in zircon, ilmenite, and monazite with normalized ion counts for comparison.

Quantitatively determined composition of zircon															
Sample		**ZrO_2**	**SiO_2**	**FeO**	**CaO**	**Al_2O_3**	**Y_2O_3**	**Ce_2O_3**	**Zr^{4+}**	**Si^{4+}**	**Fe^{2+}**	**Ca^{2+}**	**Al^{3+}**	**Y^{3+}**	**Ce^{3+}**
BA-CNS-2/1	n = 10	63,64	28,76	0,04	0,01	0,09	0,03	0,03	4,14	3,84	0,00	0,00	0,01	0,00	0,00
BA-CNS-2/2	n = 12	64,26	28,16	0,06	0,01	0,08	0,00	0,03	4,22	3,77	0,01	0,00	0,01	0,00	0,00
BL-CNS-2	n = 10	66,03	29,46	0,07	0,00	0,00	0,00	0,06	4,17	3,82	0,01	0,00	0,00	0,00	0,00
BL-CNS-3/1	n = 7	62,40	26,82	0,00	0,00	0,00	0,03	0,03	4,25	3,75	0,00	0,00	0,00	0,00	0,00
BL-CNS-3/2	n = 12	63,02	28,12	0,04	0,02	0,02	0,09	0,02	4,17	3,82	0,00	0,00	0,00	0,01	0,00
BL-CNS-3/3	n = 7	64,36	28,68	0,02	0,02	0,02	0,00	0,02	4,18	3,82	0,00	0,00	0,00	0,00	0,00
Quantitatively determined composition of ilmenite															
Sample		**FeO**	**TiO_2**	**Al_2O_3**	**MgO**	**SiO_2**	**MnO**	**CaO**	**Fe^{2+}**	**Ti^{4+}**	**Al^{3+}**	**Mg^{2+}**	**Si^{4+}**	**Mn^{2+}**	**Ca^{2+}**
BA-CNS-1	n = 10	44,86	46,17	1,82	1,45	0,90	0,81	0,02	1,77	1,61	0,31	0,10	0,21	0,03	0,00
BA-CNS-2	n = 12	34,14	55,72	0,26	0,02	0,24	3,54	0,00	1,47	2,16	0,02	0,00	0,01	0,15	0,00
BL-CNS-2/1	n = 10	39,26	55,69	0,10	0,00	0,04	4,93	0,00	1,62	2,07	0,01	0,00	0,00	0,21	0,00
BL-CNS-2/2	n = 7	42,29	55,37	0,12	0,00	0,06	4,48	0,00	1,73	2,03	0,01	0,00	0,00	0,19	0,00
Quantitatively determined composition of monazite															
Sample		**Ce_2O_3**	**La_2O_3**	**P_2O5**	**Al_2O_3**	**SiO_2**	**CaO**	**FeO**	**Ce^{3+}**	**La^{3+}**	**P^{5+}**	**Al^{3+}**	**Si^{4+}**	**Ca^{2+}**	**Fe^{2+}**
BA-CNS-1	n = 4	37,64	29,34	84,25	0,21	1,78	0,20	0,02	0,90	0,71	5,25	0,03	0,20	0,02	0,00
BL-CNS-2	n = 4	54,14	37,80	96,48	0,03	1,74	0,07	0,06	1,22	0,86	5,06	0,00	0,11	0,00	0,00
		Major oxides, weight percent							**Normalization on the basis of 16 oxygen**						

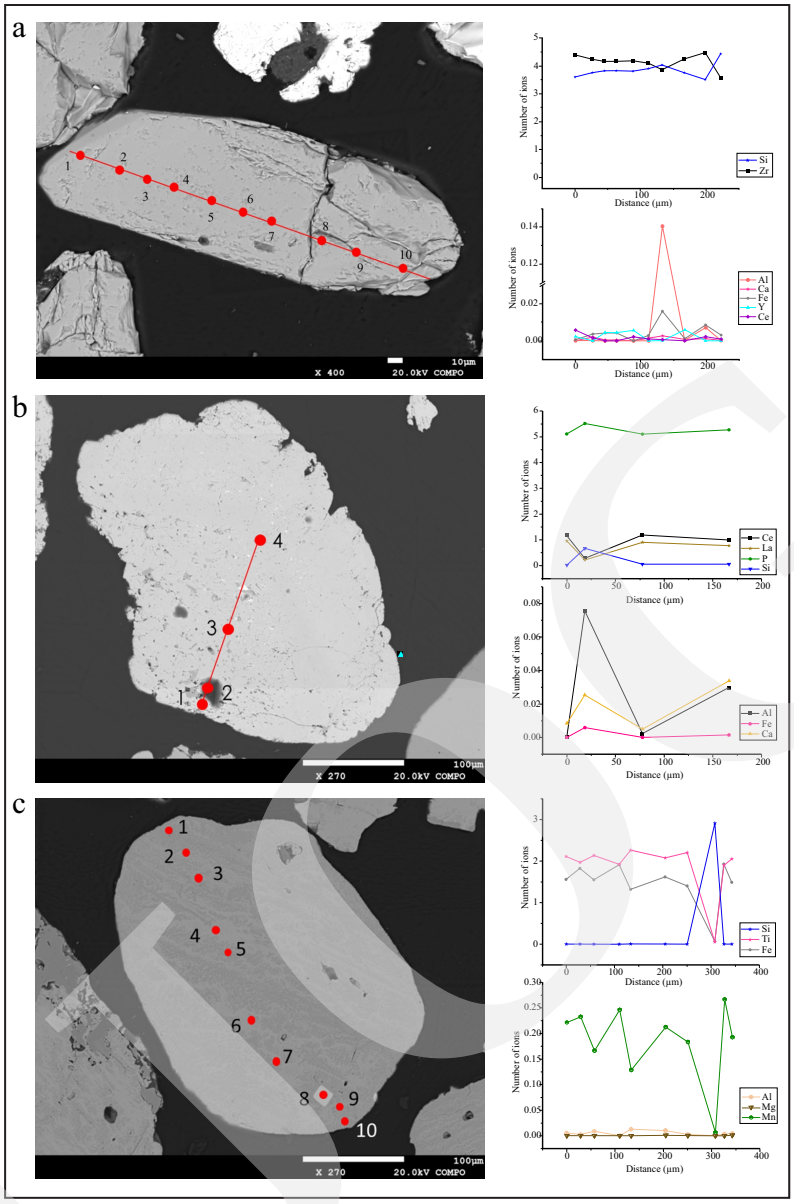

Figure 6. Atoms per formula unit (a.p.f.u) section of minerals analyzed by EPMA: (a) Zircon (BA-CNS-2), (b) Monazite (BA-CNS-1), and (c) Ilmenite (BL-CNS-2).

highly variable at about 40.78 % wt. and 55.53 % wt., respectively.

ICP-MS Analysis

To evaluate REE contents, the most representative samples were analyzed for their chemical composition through ICP-MS. A total of fourteen REE elements were analyzed: La, Ce, Pr, Nd, Sm, Eu, Gd, Tb, Dy, Ho, Er, Tm, Yb, and Lu. The highest REE content has been found in the concentrate samples (Figure 7a). The highest REEs content is 117,672 ppm of southern Bangka samples (BA-CNS-1) and 49,986.6 ppm of Belitung samples (BL-CNS-2), all of which are dominated by Ce, La, and Nd. The concentration of REEs in most of the samples exceeds the average values for the upper continental crust (UCC) (Taylor and McLennan, 1995), with enrichment factors ranging from slightly over 1 to 1,000 times, highlighting the significant REE potential of the region (Figure 7b). Whereas the tailing samples from southern Bangka and Belitung are poor in REEs: BA-TL-2 (85 ppm) and BL-TL-2 (37 ppm). The total LREE content of southern

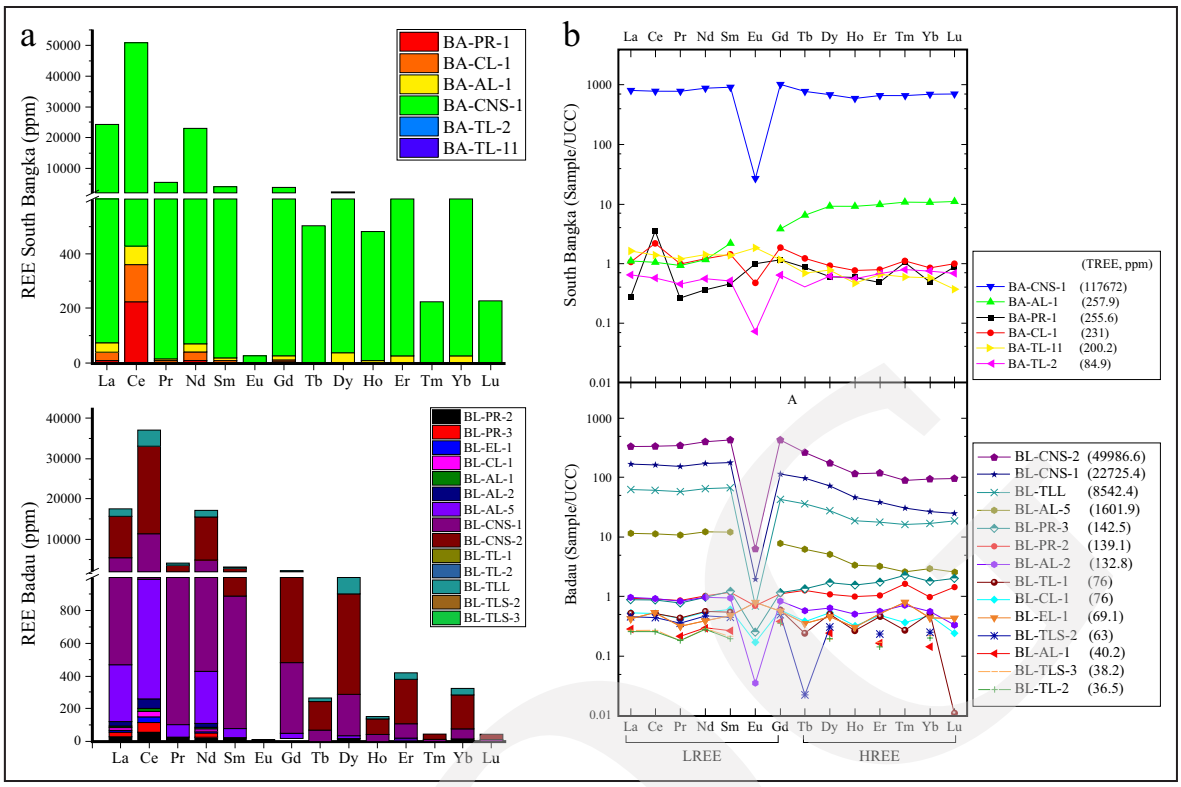

Figure 7. (a) REE concentrations and (b) UCC-normalized REE patterns (Taylor and McLennan, 1995) of primary, alluvial, concentrate, and tailing from southern Bangka and Belitung samples.

Bangka and Belitung samples showed that the predominant LREE accumulation was higher than HREE accumulation. The LREE enrichment is always greater than HREE (Table 5) where the highest LREE/HREE are 43 times at BL-CNS-1 and 42 times BA-PR-1, and the lowest LREE/HREE are 7 times at BL-PR-3 and 2 times at BA-AL-1. The LREE dominance are Ce, La, Nd, Pr, Sm, Gd, and Eu, respectively. Meanwhile, the HREE dominance are Dy, Yb, Er, Tb, Ho, Lu and Tm, respectively.

UCC-normalized shows Ce and Eu anomalies (Figure 7b). The primary sample (BA-PR-1) shows a positive Ce anomaly, extremely. Ce as an LREE has large ion radii making it incompatible (mobile), particularly in late stages of magma in the oxidation environment, enriched by that changes of Ce^{3+} to Ce^{4+} which is being stable in the crystallization process (Balaram, 2019; Hoshino *et al.*, 2016). A positive Ce anomaly is confirmed when monazite-Ce is abundant (Hoshino *et al.*, 2016). By contrast, Eu has a significantly negative anomaly. The depleted Eu is caused by redox magma during crystallization in a reduced environment. Trivalent Eu^{3+} is reduced to Eu^{2+}, while the fractionated residual granitic magma will have a negative anomaly (Linnen *et al.*, 2012; Lukanin and Dernov-Pegarev, 2010). Sample BL-TLS-2 exhibited an extreme negative Tb anomaly, a feature not observed in other samples. While this could potentially indicate unique geochemical processes or mineralogical controls within this specific tailing sample, the possibility of an analytical error or sample heterogeneity can not be excluded. Further investigation would be required to definitively determine the cause of this anomaly.

Discussions

This study comprehensively analyzes cassiterite-associated minerals in the Bangka-Belitung Islands, highlighting monazite-(Ce) and xenotime

Table 5. Concentration of REEs from Southern Bangka and Belitung Samples

Sample	BA-PR-1	BA-CL-1	BA-AL-1	BA-CNS-1	BA-TL-2	BA-TL-11	BL-PR-2	BL-PR-3	BL-EL-1	BL-CL-1
La	8.34	31.86	32.93	24169.80	19.27	48.26	27.77	26.71	12.67	15.84
Ce	222.77	138.44	66.77	50259.90	36.56	88.12	57.97	56.68	34.36	33.12
Pr	1.88	6.92	6.53	5545.73	3.24	8.50	6.03	5.62	2.24	3.03
Nd	9.35	31.05	30.08	22845.13	14.44	36.56	26.16	25.38	10.21	14.15
Sm	2.06	6.35	9.79	4100.15	2.31	6.14	5.33	5.50	2.14	2.69
Eu	0.87	0.42	nd	23.76	0.06	1.61	0.62	0.22	0.70	0.15
Gd	4.36	7.03	14.45	3870.88	2.43	4.36	4.22	4.48	2.11	2.25
Tb	0.55	0.78	4.12	498.10	0.26	0.44	0.82	0.89	0.22	0.24
Dy	2.10	3.21	32.19	2395.37	2.14	2.71	3.79	6.13	1.62	1.87
Ho	0.47	0.61	7.29	473.81	0.44	0.37	0.80	1.28	0.24	0.26
Er	1.12	1.81	22.81	1521.35	1.57	1.51	2.40	4.15	1.19	1.11
Tm	0.34	0.36	3.61	219.50	0.26	0.20	0.55	0.76	0.26	0.12
Yb	1.08	1.86	23.76	1524.84	1.65	1.27	2.15	4.08	0.98	1.06
Lu	0.28	0.32	3.57	224.41	0.22	0.12	0.46	0.66	0.14	0.08
Ce/Ce*	13.80	2.29	1.12	1.06	1.13	1.07	1.18	1.15	1.89	1.55
Eu/Eu*	0.89	0.19	-	0.02	0.08	0.95	0.40	0.14	1.00	0.19
ΣLREE (ppm)	249.63	222.07	160.55	110815.34	78.31	193.54	128.10	124.60	64.43	71.22
ΣHREE (ppm)	5.93	8.95	97.34	6857.38	6.55	6.62	10.97	17.94	4.66	4.74
ΣREE (ppm)	255.56	231.01	257.89	117672.72	84.86	200.16	139.07	142.54	69.08	75.96
LREE/HREE	42.09612	24.81229	1.649373	16.16001	11.95573	29.23565	11.6773	6.945373	13.82618	15.02532
Sample	**BL-AL-1**	**BL-AL-2**	**BL-AL-8**	**BL-CNS-1**	**BL-CNS-2**	**BL-TL-1**	**BL-TL-2**	**BL-TLL**	**BL-TLS-2**	**BL-TLS-3**
La	8.56	29.23	348.50	5009.23	10172.00	15.70	7.80	1867.24	13.61	8.12
Ce	18.26	58.79	730.56	10382.64	21746.14	33.63	16.43	3882.17	28.30	17.35
Pr	1.53	5.87	77.24	1084.45	2477.65	3.08	1.31	412.24	2.55	1.32
Nd	7.66	25.53	319.62	4485.78	10566.84	14.49	7.29	1686.64	12.42	7.49
Sm	1.20	4.25	55.25	810.62	1954.56	2.46	0.89	304.07	2.02	0.96
Eu	nd	0.03	nd	1.74	5.59	nd	nd	0.61	nd	nd
Gd	1.46	3.20	30.03	435.81	1646.42	2.21	1.34	163.41	1.89	1.35
Tb	nd	0.37	4.03	61.84	172.48	0.16	nd	23.17	0.01	nd
Dy	0.85	2.24	18.11	250.45	614.30	1.73	0.69	97.62	1.08	0.68
Ho	nd	0.41	2.75	37.05	92.25	0.21	nd	15.18	nd	nd
Er	0.38	1.30	7.55	88.58	271.72	1.06	0.33	41.18	0.54	0.40
Tm	nd	0.24	0.87	10.07	29.59	0.09	nd	5.39	nd	nd
Yb	0.32	1.23	6.60	59.16	206.25	1.14	0.44	37.47	0.56	0.48
Lu	nd	0.11	0.84	8.04	30.79	0.00	nd	6.03	nd	nd
Ce/Ce*	-	2.22	1.04	1.25	0.96	25.70	-	0.89	-	-
Eu/Eu*	-	0.03	-	0.01	0.01	-	-	0.01	-	-
ΣLREE (ppm)	38.67	126.89	1561.19	22210.26	48569.20	71.57	35.06	8316.38	60.79	36.60
ΣHREE (ppm)	1.55	5.89	40.75	515.18	1417.38	4.40	1.46	226.04	2.20	1.56
ΣREE (ppm)	40.22	132.78	1601.94	22725.44	49986.58	75.97	36.52	8542.42	62.98	38.16
LREE/HREE	24.94839	21.54329	38.31141	43.11165	34.26689	16.26591	24.0137	36.79163	27.63182	23.46154

nd: not detected

as the primary carriers of LREEs and HREEs, respectively. These findings emphasize the importance of these minerals in the local mineralogical landscape. The detailed mineralogical analysis revealed that monazite is more abundantly present and is particularly enriched in LREEs such as Ce, La, and Nd. While less abundant, xenotime hosts critical HREEs, including Y, Dy, and Yb. This distribution correlates with their known geochemical behaviours in granitic and hydrothermal systems and aligns with the observed LREE enrichment across different sample types, reflecting

their compatibility with the residual melt during magmatic differentiation (Chakhmouradian and Wall, 2012).

The distribution of monazite and xenotime across different deposit types and size fractions provides insights into their behaviour during mineral processing and their potential for recovery. As seen in the mineralogical analyses (Table 2), monazite is prevalent in concentrates from both Bangka and Belitung, indicating its concentration alongside cassiterite during processing. Interestingly, there is a weak positive correlation between cassiterite and monazite abundance, suggesting that their occurrence and enrichment are influenced by similar factors. This could be related to their shared origin within granitic rocks or their comparable behaviours during weathering and sedimentary transport. In contrast, xenotime tends to be found in finer-size fractions, as shown by SEM and XRD analyses, suggesting its potential loss during certain processing stages or its association with finer-grained minerals.

Ilmenite and zircon are also prominent within these deposits, each exhibiting varying relationships with cassiterite depending on the location and sample type. Ilmenite, valued for its titanium content, adds economic potential to the mineral deposits. In southern Bangka, a weak negative correlation is observed between cassiterite and ilmenite abundance, suggesting that factors influencing their enrichment may differ or that they respond differently to mineral processing techniques. However, in Belitung, a weak positive correlation suggests that their occurrence is linked, potentially due to shared geological controls or similar behaviour during sedimentary processes. Zircon, though commonly a carrier of REEs in other contexts (Long *et al*., 2012), does not exhibit significant REE content in this specific setting. However, its presence shows a location-dependent relationship with cassiterite. In southern Bangka, a negative correlation is observed, whereas Belitung samples display a weak positive correlation. These varying correlations highlight the complexity of mineral associations within the cassiterite deposits, and suggest the influence of local geological factors and processing methods on mineral distribution patterns.

The granitic settings of the Bangka-Belitung region, part of the extensive Southeast Asian Tin Belt, provide a rich geochemical environment where the processes of magmatic differentiation and subsequent hydrothermal activity contribute to the formation and accumulation of these minerals (Ng *et al*., 2017). The differential weathering resistance of monazite and xenotime significantly influences their enrichment in placer deposits, as these minerals resist breakdown more effectively than other REE-bearing minerals, leading to their accumulation in secondary deposit formations (Kudrass, 2016).

The presence of REE-rich monazite and xenotime within the cassiterite-associated mineral deposits (Table 3) offers considerable economic opportunities for extracting these elements alongside traditional tin mining practices in Bangka and Belitung. The substantial concentrations of LREEs in the Bangka concentrate samples (with REE contents reaching up to 117,672 ppm in some concentrates) suggest a promising economic opportunity for the region. However, the extraction processes must address the environmental challenges posed by the high thorium content in monazite. This necessitates the development of processing technologies that can effectively separate and manage radioactive waste to mitigate environmental and health risks (International Atomic Energy Agency, 2002; Zglinicki *et al*., 2021).

The global dynamics of the REE market, including demand fluctuations and geopolitical influences, further complicate the economic landscape. The need for sustainable and responsible mining practices is paramount to minimize the ecological footprint of REE mining. Innovative technologies that enhance the efficiency of REE extraction and reduce the environmental impact are crucial for the long-term viability of this sector. Future research should focus more on the mechanisms of REE partitioning between monazite and xenotime, and the factors influencing their geochemical behaviour in different granitic

environments. Comparative analyses with other global deposits could provide valuable insights into the geochemical variability of REE-bearing minerals, and inform better exploration and processing strategies. Understanding the environmental impacts of thorium and other radioactive elements associated with REE mining is essential for developing effective mitigation strategies.

Conclusions

This study investigated the REE potential within the cassiterite-associated minerals in Bangka-Belitung Islands. Through microscopy and XRD analyses, it is identified that monazite and xenotime as the primary REE-bearing minerals, with their dominance particularly evident in concentrate samples. Other minerals commonly associated with cassiterite, such as ilmenite and zircon, were also observed but lacked significant REE content. SEM analysis revealed monazite-(Ce) as the most prominent REE-bearing mineral, often containing huttonite inclusions and enriched in Ce, La, and Nd. Xenotime, though less abundant, hosted HREEs like Y, Dy, and Yb. ICP-MS analysis confirmed the dominance of monazite and the overall enrichment of light REEs (LREEs) over heavy REEs (HREEs), highlighting the potential of these regions for LREE exploration and resource development. However, the presence of radioactive elements, particularly thorium within monazite, necessitates careful consideration for responsible and sustainable extraction practices.

Acknowledgments

The authors thank Teti Indriati and Andy Yahya Al Hakim for their assistance in the interpretation and discussion of the mineralogical analysis. Thanks go to Kotaro Yonezu from Kyushu University and Ryohei Takahashi from Akita University for access to the SEM-EDS, EPMA, and ICP-MS facilities. The authors also thank Periska Rasma and Enrico Gilrandy for their support during fieldwork and the administrative process. This work was supported by P.T. Timah Tbk., and funded by Institut Teknologi Bandung through Research, Community Service, and Innovation program (PPMI – ITB), and Ministry of Education, Culture, Research, and Technology through Basic Research program (PDUPT – Kemendikbud/Ristek).

References

Akagi, T., Fu, F., Hongo, Y., and Takahashi, K., 2011. Composition of rare earth elements in settling particles collected in the highly productive North Pacific Ocean and Bering Sea: Implications for siliceous-matter dissolution kinetics and formation of two REE-enriched phases. *Geochimica et Cosmochimica Acta,* 75 (17), p.4857-4876. DOI:10.1016/j.gca.2011.06.001.

Aryanto, N.C.D. and Kamiludin, U., 2016. The Content of Placer Heavy Mineral and Characteristics of REE at Toboali Coast and Its Surrounding Area, Bangka Belitung Province. *Bulletin of the Marine Geology,* 31 (1), p.45-54. DOI:10.32693/bomg.31.1.2016.318.

Baharrudin and Sidarto, 1995. *Geological Map of Belitung Sheet, Sumatera, Scale 1:250,000*. Geological Research and Development Centre, Bandung.

Balaram, V., 2019. Rare earth elements: A review of applications, occurrence, exploration, analysis, recycling, and environmental impact. *Geoscience Frontiers,* 10 (4), p.1285-1303. DOI:10.1016/J.GSF.2018.12.005.

Barakos, G., Gutzmer, J., and Mischo, H., 2016. Strategic evaluations and mining process optimization towards a strong global REE supply chain. *Journal of Sustainable Mining,* 15 (1), p.26-35. DOI:10.1016/j.jsm.2016.05.002.

Chakhmouradian, A.R. and Wall, F., 2012. Rare Earth Elements: Minerals, Mines, Magnets (and More). *Elements*, 8 (5), p.333-340. DOI:10.2113/gselements.8.5.333.

Cobbing, E.J., Mallick, D.I.J., Pitfield, P.E.J., and Teoh, L.H., 1986. The granites of the South-east Asian Tin Belt. *Journal of Geological Society,* 143 (3), p.537-550. DOI:10.1144/gsjgs.143.3.0537.

Connelly, N.G., Hartshorn, R.M., Damhus, T., and Hutton, A.T., 2005. *Nomenclature of Inorganic Chemistry IUPAC Recommendations.* The Royal Society of Chemistry.

Firdaus, M.A., Hede, A.N.H., Syafrizal, S., and Heriawan, M.N., 2020. Exploring Spectral Reflectance to Identify Rare Earth Element-Bearing Minerals Associated with Alluvial Tin Deposits. *International Symposium on Earth Science and Technology,* Fukuoka, Japan.

Gosen, B.S. van, Verplanck, P.L., Seal II, R.R., Long, K.R., and Gambogi, J., 2017. Rare-earth elements, Chapter O, (eds), Critical mineral resources of the United States—Economic and environmental geology and prospects for future supply. U.S. Geological Survey, Professional Paper 1802, p.O1-O31. DOI:10.3133/pp1802O.

Haque, N., Hughes, A., Lim, S., and Vernon, C., 2014. Rare Earth Elements: Overview of Mining, Mineralogy, Uses, Sustainability and Environmental Impact. *Resources,* 3 (4), p.614-635. DOI:10.3390/resources3040614.

Hoshino, M., Sanematsu, K., and Watanabe, Y., 2016. Chapter 279 - REE Mineralogy and Resources. *In*: Jean-Claude, B. and Vitalij, K.P, (eds.), *Handbook on the Physics and Chemistry of Rare Earths*. Elsevier, 49, p.129-291. DOI:10.1016/bs.hpcre.2016.03.006.

Indonesia, 2020. *Law of the Republic of Indonesia No. 11 of 2020 on Job Creation*, Kementerian Sekretariat Negara Republik Indonesia.

International Atomic Energy Agency, 2002. Management of Radioactive Waste from the Mining and Milling of Ores. *IAEA Safety Standards Series,* WS-G-1.2, *Vienna*.

Irzon, R., 2021. REE-Bearing Minerals in Tin Waste Dumps of Singkep Island: Geochemical Identification and Recovery. *Indonesian Journal on Geoscience,* 9 (1), p.15-26. DOI:10.17014/ijog.9.1.15-26.

Irzon, R., Syafri, I., Hutabarat, J., and Sendjaja, P., 2016. REE Comparison Between Muncung Granite Samples and their Weathering Products, Lingga Regency, Riau Islands. *Indonesian Journal on Geoscience,* 3 (3), p.149-161. DOI:10.17014/ijog.3.3.149-161.

Jones, M.T., Reed, B.L., Doe, B.R., and Lanphere, M.A., 1977. Age of tin mineralization and plumbotectonics, Belitung, Indonesia. *Economic Geology,* 72 (5), p.745-752. DOI:10.2113/gsecongeo.72.5.745.

Kelly, N. M., Harley, S. L., and Moller, A., 2012. Complexity in the behavior and recrystallization of monazite during high-T metamorphism and fluid infiltration. *Chemical Geology,* 322-323, p.192-208. DOI:10.1016/j.chemgeo.2012.07.001.

Kudrass, H., 2016. Formation of Placer Deposits, *in*: *Reference Module in Earth Systems and Environmental Sciences*. Elsevier. DOI:10.1016/b978-0-12-409548-9.09233-2.

Linnen, R.L., Van Lichtervelde, M., and Černý, P., 2012. Granitic Pegmatites as Sources of Strategic Metals. *Elements*, 8 (4), p.275-280. DOI:10.2113/gselements.8.4.275.

Long, K.R., Gosen, B.S. van, Foley, N.K., Cordier, D., and Vertaq, S., 2012. The principal rare earth elements deposits of the United States: A summary of domestic deposits and a global perspective. *In*: Sinding-Larsen, R., and Wellmer, F.W. (eds.), *Non-Renewable Resource Issues*. International Year of Planet Earth. Springer, Dordrecht, p.131-155. DOI:10.1007/978-90-481-8679-2_7.

Lukanin, O.A. and Dernov-Pegarev, V.F., 2010. Partitioning of rare earth elements between an aqueous chloride fluid phase and melt during the decompression-driven degassing of granite magmas. *Geochemistry International,* 48, p.961-978. DOI:10.1134/S0016702910100022.

Margono, U., Supandjono, R.J.B., and Partoyo, E., 1995. *Geological Map of the South Bangka Sheet, Sumatera, Scale 1:250,000*. Geological Development and Research Centre, Bandung.

Maulana, A., Sanematsu, K., and Sakakibara, M., 2016. An Overview on the Possibility of Scandium and REE Occurrence in Sulawesi, Indonesia. *Indonesian Journal on Geoscience,* 3 (2), p.139-147. DOI:10.17014/ijog.3.2.139-147.

Mcbeth, J., 2020. *Race is on for Indonesia's untapped rare earths*. https://asiatimes.com/2020/09/race-is-on-for-indonesias-untapped-rare-earths/ [28 April 2024].

Mos, Y.M., Vermeulen, A.C., Buisman, C.J.N., and Weijma, J., 2018. X-Ray Diffraction of Iron Containing Samples: The Importance of a Suitable Configuration. *Geomicrobiology Journal*, 35 (6), p.511-517. DOI:10.1080/01490451.2017.1401183.

Ng, S.W.P., Whitehouse, M.J., Roselee, M.H., Teschner, C., Murtadha, S., Oliver, G.J.H., Ghani, A.A., and Chang, S.C., 2017. Late Triassic granites from Bangka, Indonesia: A continuation of the Main Range granite province of the South-East Asian Tin Belt. *Journal of Asian Earth Sciences,* 138, p.548-561. DOI:10.1016/j.jseaes.2017.03.002.

Purwadi, I., Werff, H. van der, and Lievens, C., 2019. Reflectance spectroscopy and geochemical analysis of rare earth element-bearing tailings: A case study of two abandoned tin mine sites in Bangka Island, Indonesia. *International Journal of Applied Earth Observation and Geoinformation,* 74, p.239-247. DOI:10.1016/J.JAG.2018.09.006.

Riebe, C.S., Kirchner, J.W., Granger, D.E., and Finkel, R.C., 2001. Strong tectonic and weak climatic control of long-term chemical weathering rates. *Geology,* 29 (6), p.511-514. DOI:10.1130/0091-7613(2001)029<0511:STAWCC>2.0.CO;

Sanematsu, K. and Watanabe, Y., 2016. Characteristics and Genesis of Ion Adsorption-Type Rare Earth Element Deposits. *In*: Verplanck, P.L. and Hitzman, M.W. (eds.), Rare Earth and Critical Elements in Ore Deposits. *Society of Economic Geologists,* 18. DOI:10.5382/Rev.18.03.

Schwartz, M.O., Rajah, S.S., Askury, A.K., Putthapiban, P., and Djaswadi, S., 1995. The Southeast Asian tin belt. *Earth Science Reviews,* 38 (2-4), p.95-293. DOI:10.1016/0012-8252(95)00004-T.

Schwartz, M.O. and Surjono, 1991. The Pemali tin deposit, Bangka, Indonesia. *Mineralium Deposita*, 26, p.18-25. DOI:10.1007/BF00202359.

Schwartz, M.O. and Surjono, 1990. Greisenization and albitization at the Tikus tin-tungsten deposit, Belitung, Indonesia. *Economic Geology,* 85 (4), p.691-713. DOI:10.2113/gsecongeo.85.4.691.

Sengupta, D. and Gosen, B.S. van, 2016. Placer-Type Rare Earth Element Deposits. *In*: Verplanck, P.L., and Hitzman, M.W. (eds.), Rare Earth and Critical Elements in Ore Deposits. *Society of Economic Geologists,* 18. DOI:10.5382/rev.18.04.

Suprapto, S.J., 2009. Tinjauan Tentang Unsur Tanah Jarang. *Buletin Sumber Daya Geologi,* 4 (1), p.36-47. DOI:10.47599/bsdg.v4i1.173.

Syafrizal, Indriati, T., Hede, A.N.H., and Muhammad, A., 2017. Mineralogical Analyses as a Preliminary Assessment of Rare Earth Elements on Placer Deposits in Belitung Island, Indonesia. *International Symposium On Earth Science and Technology*, Fukuoka, Japan.

Szamałek, K., Konopka, G., Zglinicki, K., and Marciniak-Maliszewska, B., 2013. New potential source of rare earth elements. *Gospodarka Surowcami Mineralnymi-mineral Resources Management,* 29 (4), p.59-76. DOI:10.2478/gospo-2013-0041.

Taylor, S.R. and McLennan, S.M., 1995. The geochemical evolution of the continental crust. *Reviews of Geophysics,* 33 (2), p.241-265. DOI:10.1029/95RG00262.

USGS, 2021. Mineral commodity summaries 2021, *Mineral Commodity Summaries*. U.S. Geological Survey, Reston, VA. DOI:10.3133/mcs2021.

Yaraghi, A., Ariffin, K.S., and Baharun, N., 2020. Comparison of characteristics and geochemical behaviors of REEs in two weathered granitic profiles generated from metamictized bedrocks in Western Peninsular Malaysia.

Journal of Asian Earth Sciences, 199. DOI:10.1016/j.jseaes.2020.104385.

Zglinicki, K., Małek, R., Szamałek, K., and Wołkowicz, S., 2022. Mining Waste as a Potential Additional Source of HREE and U for the European Green Deal: A Case Study of Bangka Island (Indonesia). *Minerals,* 12 (1), 3333344. DOI:10.3390/min12010044.

Zglinicki, K., Szamałek, K., and Wołkowicz, S., 2021. Critical Minerals from Post-Processing Tailing. A Case Study from Bangka Island, Indonesia. *Minerals*, 11 (4), 352. DOI:10.3390/min11040352.

Zhou, B., Li, Z., and Chen, C., 2017. Global Potential of Rare Earth Resources and Rare Earth Demand from Clean Technologies. *Minerals,* 7 (11), 203. DOI:10.3390/min7110203.

IJOG